AIAA 2004-1574

New Deployable Reflector Concept

O. Soykasap , A.M. Watt , and S. Pellegrino
University of Cambridge, Cambridge, CB2 1PZ, UK

45th AIAA/ASME/ASCE/AHS/ASC Structures, Structural Dynamics, and Materials Conference
19-22 April 2004
Palm Springs, CA

New Deployable Reflector Concept

Ö. Soykasap*, A.M. Watt†, and S. Pellegrino‡
University of Cambridge, Cambridge, CB2 1PZ, UK

This paper presents a new deployable reflector concept for an Earth observation mission that requires a low-cost L-band Synthetic Aperture Radar (SAR) instrument using an offset parabolic cylinder with a linear feed array. The required reflector shape is an offset parabolic cylinder with arc-length of 7.9 m and width of 3.2 m. A novel "hollow solid" structural concept is proposed that comprises curved surfaces formed from thin sheets of carbon-fiber-reinforced-plastic (CFRP) connected by flexible hinges along the edges. The front surface of the hollow solid has the required shape for the reflector. This proposed structure has very high stiffness-to-mass-ratio, because of its thin-walled box-type construction. A detailed study of a half-scale technology demonstrator, including design, manufacture and testing is presented in the paper. A preliminary design of the full-scale structure, which has an estimated mass of 33 kg, is also presented.

Introduction

New structural concepts for large deployable spacecraft structures are currently being developed to meet the needs of low cost missions using small satellites. General requirements include the ability to deploy large surfaces in space (flat or curved, depending on the mission) using structures of low mass and of sufficient stiffness that there is no dynamic coupling between the structure and the attitude control system of the spacecraft. It is also required that these structures stow in a compact volume, and deploy reliably to the correct shape. Current efforts towards lowering the cost of these structures aim to reduce the number of parts required to manufacture them, and also to reduce the complexity of making, assembling and testing these parts.

This paper presents a novel deployable reflector structure, for a mission requiring a low-cost L-band Synthetic Aperture Radar (SAR) instrument using an offset parabolic cylinder with a linear feed array. The satellite is designed to perform low-cost Earth observation missions; a schematic diagram of the flight configuration is shown in Figure 1. This configuration provides some of the advantages of phased arrays (like low loss and elevation beam steering), at much reduced cost. The required reflector shape is an offset parabolic cylinder with an arc-length of 7.9 m and width of 3.2 m. Note that the reflector structure is connected to the spacecraft bus by a truss structure, which would be deployed before the reflector structure itself. This structure will not be investigated here.

A low-risk solution for the reflector structure would be to use four lightweight, curved sandwich panels, connected by self-locking hinges [1]. The mass of this structure was estimated at 79 kg by EADS Astrium.

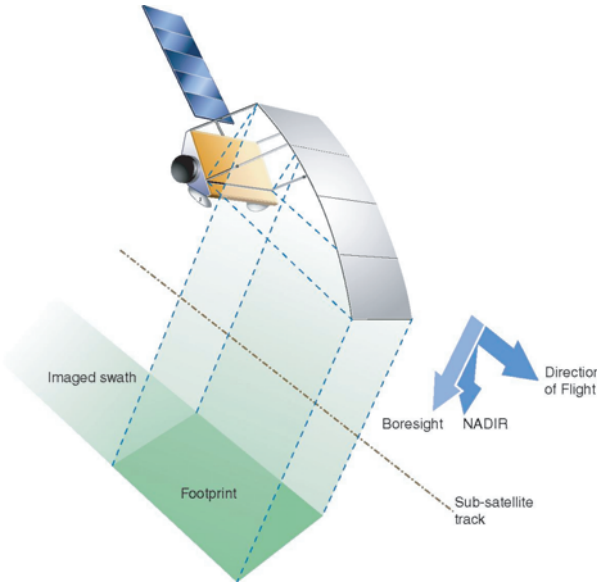

Fig. 1 Flight configuration (courtesy of EADS Astrium).

This paper presents an alternative, much lighter concept. The idea is to form a "hollow solid" from thin, curved sheets of carbon-fiber-reinforced-plastic (CFRP), connected by flexible hinges along the edges, which forms continuous reflective surface that has the required shape for the reflector.

This structure has very high stiffness-to-mass-ratio, because of its thin-walled box-type construction. Only minimal use of stiffening elements is required, as the curvature of each surface is an effective way of increasing the local buckling stress of a very thin sheet.

A brief outline of the paper is as follows. The section Structural Concept explains the proposed approach and the section Cutting Pattern derives the cutting

*Research Associate, Department of Engineering, Trumpington Street. Member AIAA.

†Research Associate, Department of Engineering, Trumpington Street.

‡Professor of Structural Engineering, Department of Engineering, Trumpington Street. Associate Fellow AIAA.

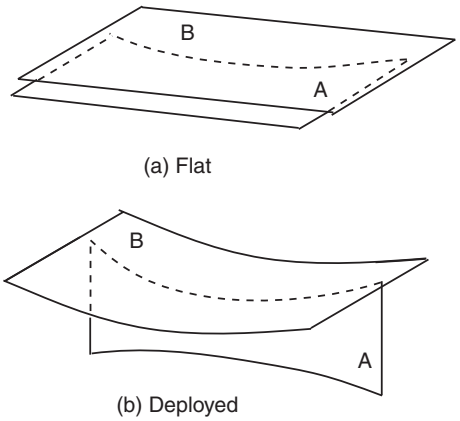

Fig. 2 Use of a shaped sheet A to form sheet B into a singly-curved surface.

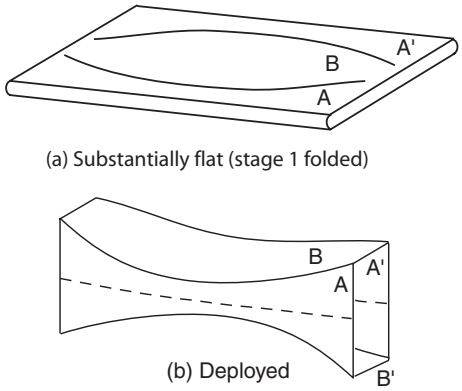

Fig. 3 Hollow solid structure.

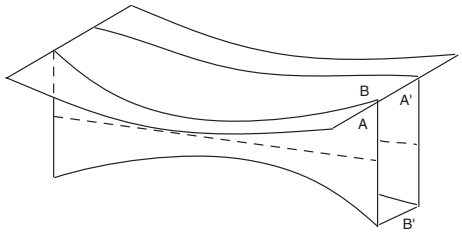

Fig. 4 Antenna structure in deployed configuration.

pattern for the four sheets that make up the structure. Then, the sections Design for Folding and Design of Reflector Structure outline the key stages of the design process of this novel structure, including the constraints imposed by the requirement to elastically fold the structure, the design of a half-scale technology demonstrator, and the preliminary design of a full-scale flight structure. A key parameter is the minimum bend radius of the thin CFRP sheets that make up the structure; this is obtained by direct measurement, and is also estimated analytically. Detailed finite-element analyses of the static and dynamic behaviour of both half-scale and full-scale structures are obtained. The construction and laboratory testing of the half-scale demonstrator are presented. A Discussion concludes the paper.

Structural Concept

The key geometric ideas behind the proposed new concept can be explained as follows.

Consider a flat sheet A with a curved edge, connected to a coplanar flat sheet B, as shown in Figure 2(a). If sheet A is rotated through 90°, both sheets become curved, as shown in Figure 2(b).

Next consider the "hollow-solid" structure shown in Figure 3, made by connecting two pairs of identical flat sheets. Sheets A and A', which are identical, are connected to sheets B and B', also identical. The shape of the curved edges is identical in all four sheets. In the configuration shown in Figure 3(b) the four sheets form curved surfaces which define a hollow solid whose shape is defined by the cutting pattern of the sheets. The folded configuration shown in Figure 3(a) is obtained by introducing fold lines in the middle of sheets A and A' (shown as broken lines in the Figure 3(b)).

Once the hollow solid structure has been flattened (which we call stage one of the folding process) it can then be folded longitudinally (stage two of the folding process) as an accordion, or rolled up into a coil.

A reflective surface of cylindrical shape can be formed by replacing sheet B with a rectangular sheet, see Figure 4.

Next, we explain how to determine the edge profile of sheet A. Figure 5(a) shows two cylindrical surfaces, A and B, that intersect along the curve OEC. Surface B can be generated by considering the two-dimensional curve $z = d(x)$, and by translating this curve along a generator segment, e.g. LM, parallel to the y-axis. Note that in Figure 5(a) a general point on $z = d(x)$ is point D; also note that the x-axis starts at the origin O and passes through the end point C of the curve. Finally, note that all points on LM have the same arc-length distance s from the y-axis, and the same distance d from the xy plane.

Let F and G be the projections of D and E onto the xy plane, clearly

$$\overline{\mathrm{DF}} = \overline{\mathrm{EG}} = d \tag{1}$$

Now consider flattening the surface B onto the xy-plane, without moving its edge along the y-axis. During this process LM moves in the x and z directions, while remaining parallel to the y-axis. The distance d of E from the xy-plane becomes zero.

Next, we consider the additional conditions that need to be satisfied for the two surfaces to be flattened together. We look for the locus of points E on the surface B defining the curved profile of surface A, and hence the curve along which the two surfaces are attached. It will be assumed that the generator LM is perpendicular to the surface A in the curved configuration (i.e. the deployed configuration), although a more

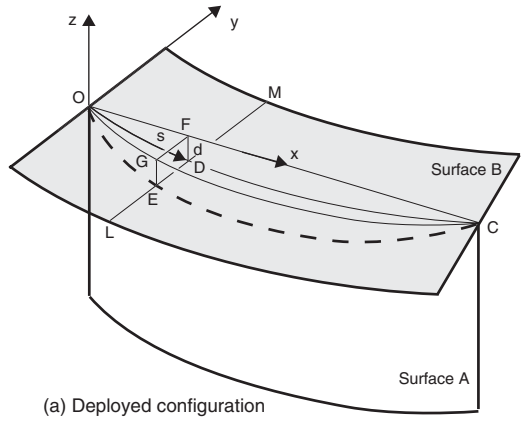

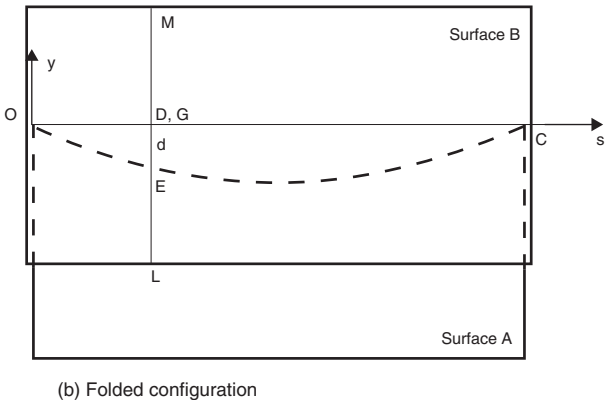

Fig. 5 Required edge profile of sheet A to shape a singly-curved surface.

general situation could be considered. It will also be assumed that the two surfaces are tied to each other at the general point E and there is no relative motion of the tie points when the surfaces are flattened.

The following conditions apply

- Condition 1: The arc-length of OE, measured on the surface B is equal to the arc-length of OE measured on the surface A. This condition needs to be satisfied in the two extreme configurations shown in Figure 5. It should be satisfied in intermediate configurations.
- Condition 2: When the surfaces are flattened, both points D and G move towards point F, and so D and G coincide when the surfaces are flattened, see Figure 5(b). Hence, it follows that

$$\overline{\mathrm{DE}} = \overline{\mathrm{EG}} = d \tag{2}$$

In conclusion, given a three-dimensional cylindrical surface (surface B) defined by a two-dimensional curve $z = d(x)$, first one has to determine the arc-length, $s(x)$, along the curve and then one has to determine the edge profile of surface A, given by $d(s)$. Note that $d(s)$ also defines the curve along which surface A is to be connected to surface B. If $d(s)$ cannot be found explicitly, then an implicit description in terms of $s(x)$ and $d(x)$ can be used instead.

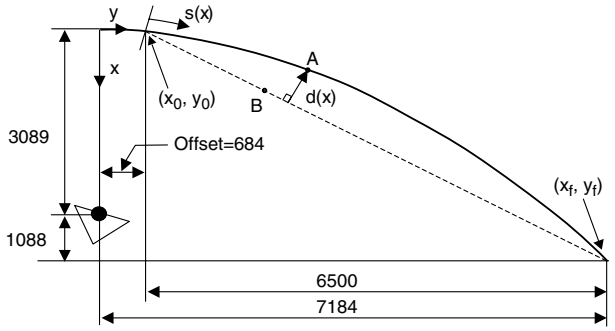

Fig. 6 Profile of RF surface (dimensions in mm).

Note that, from Equation 2, both sheets have the same singly-curved shape in the deployed configuration.

Cutting Pattern

Here we work out the cutting pattern for the sheets of a reflector structure, to provide the required focal length, aperture, and offset distance.

The required parabolic profile for the reflective surface is shown in Figure 6. The cutting pattern of the flat sheets requires the arc length $s(x)$ and the perpendicular distance from the chord line to the parabola $d(x)$ to be worked out, as discussed in previous section.

The equation of a parabola with vertex at (0, 0) is given by

$$y^2 = 4ax \tag{3}$$

where a is the focal distance. The arc length from the offset (x_0, y_0) to a generic point $\mathrm{A}(x, y)$ on the parabola, is calculated from

$$s(x) = \int_{x_0}^{x} \sqrt{1 + (dy/dx)^2}\, dx \tag{4}$$

Substituting Eq. 3 into Eq. 4 and carrying out the integration yields

$$\begin{aligned} s(x) = \quad & \sqrt{x\,(x+a)} - \sqrt{x_0\,(x_0+a)} \\ & + \frac{a}{2}\ \ln \frac{2\,x + a + 2\,\sqrt{x\,(x+a)}}{2\,x_0 + a + 2\,\sqrt{x_0\,(x_0+a)}} \end{aligned} \tag{5}$$

The equation of the chord line of the reflector, which joins the start (x_0, y_0) and end (x_f, y_f) points of the reflective surface, is written as

$$y_c = a_0 + a_1 x \tag{6}$$

where $a_0 = (y_0 x_f - x_0 y_f)/(x_f - x_0)$, and $a_1 = (y_f - y_0)/(x_f - x_0)$.

Consider a general point on the chord line, $\mathrm{B}(x_c, y_c)$. The distance between A and B is

$$d_{AB} = \sqrt{(x - x_c)^2 + (y - y_c)^2} \tag{7}$$

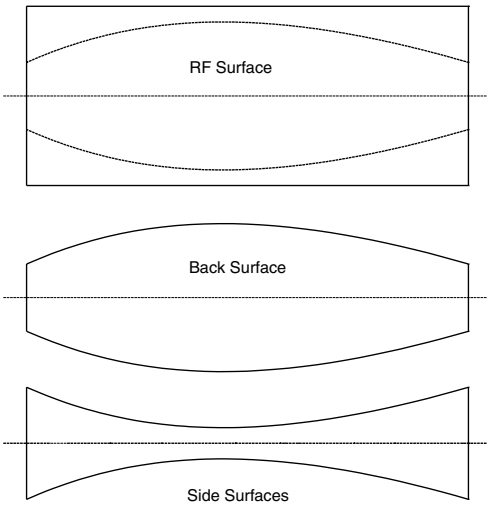

Fig. 7 Cutting pattern for reflector structure.

Substituting Eqs. 3 and 6 into Eq. 7 we obtain

$$d_{AB} = \sqrt{(x - x_c)^2 + (2\sqrt{ax} - a_0 - a_1 x_c)^2} \qquad (8)$$

The shortest distance $d(x)$ from point A to the chord line can be obtained by minimizing d_{AB}. Hence we set the first derivative of d_{AB} with respect to x_c equal to zero and solve for x_c, to obtain

$$x_c = \frac{(x + 2a_1\sqrt{ax} - a_0 a_1)}{(1 + a_1^2)} \qquad (9)$$

The shortest distance $d(x)$ is obtained by substituting Eq. 9 into Eq. 8

$$d(x) = \frac{|\,(x\,a_1 + a_0 - 2\,\sqrt{ax})\,|}{\sqrt{1 + {a_1}^2}} \qquad (10)$$

The cutting pattern for the flat sheets, defined by $s(x)$ and $d(x)$ in Eqs 5, 10, is shown in Figure 7.

Two more parameters are needed to completely determine the cutting pattern for the reflector, namely the distance between the two matching profiles in each of the four sheets that form the hollow solid. These parameters are determined by thinking about the size of the packaged structure and by optimizing the performance of the structure in the deployed configuration [2].

Design for Folding

The reflector structure is to be constructed from thin sheets of CFRP. This section presents the analysis and detailed testing of those elements of the reflector structure that need to elastically deform in order to allow folding of the structure.

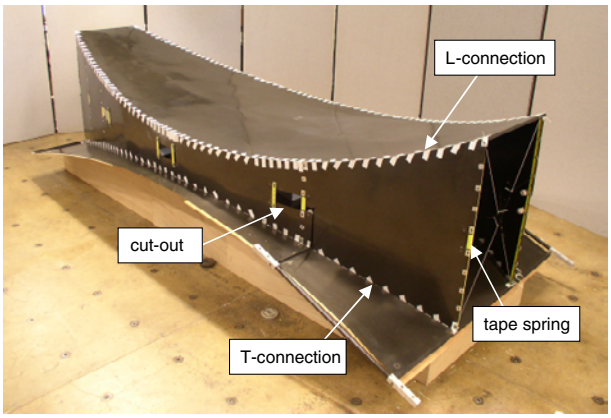

Fig. 8 Types of connection.

Connections

All connections must be strong enough to transfer the loads from one surface to another, and also flexible enough to allow folding and unfolding of the structure. Surface-to-surface connections prevent relative translation between matching points on two lines of separate sheets, but allow the sheets to rotate. Two types of connections have been used, see Figure 8. These connections have been made with adhesive tape in order to provide a uniform stress distribution across the two sheets being connected.

Elastic Hinge Lines

Elastic hinge lines are formed between parts of a sheet of CFRP that describe an essentially rigid-body rotation with respect to each other. Careful design of the parts of the structure that have to flex is required, limiting the maximum curvature to which they are subjected. In simple terms, the maximum strain imposed by the folding process has to be smaller than a threshold value, which depends on the properties of the CFRP sheet.

An elastic hinge line is made to latch in one particular configuration by fastening tape springs (i.e. lengths of steel carpenter tape) to it. Note that in Figure 8 a small part of the sheet under each tape spring has been removed to form a cut-out which provides the clearance needed for the tape springs to fold without being overstressed.

Prediction of Minimum Bend Radius

To ensure that no material failure occurs during folding of the reflector structure, the minimum bend radius of the CFRP sheets was measured experimentally, and also estimated theoretically. The estimated results were compared to the experimental results.

The maximum strain criterion assumes that failure of a laminated composite occurs when the in-plane strains along the principal material directions exceed

the ultimate strains of the material, hence [3]

$$\begin{array}{c} -\epsilon_L^{(-)} < \epsilon_1 < \epsilon_L^{(+)} \\ -\epsilon_T^{(-)} < \epsilon_2 < \epsilon_T^{(+)} \\ \mid \gamma_{12} \mid < \epsilon_{LT} \end{array} \tag{11}$$

where $\epsilon_L^{(-)}$ and $\epsilon_L^{(+)}$ are the longitudinal ultimate strains in compression and tension; $\epsilon_T^{(-)}$ and $\epsilon_T^{(+)}$ are the transverse ultimate strains in compression and tension; ϵ_{LT} is the ultimate shear strain.

Consider a flat, balanced, symmetric laminated plate, initially unstressed. A large curvature is imposed along the x-axis and, since the in-plane stiffness of the plate prevents it from stretching, the plate deforms into a purely cylindrical surface (apart from a narrow boundary-layer near the edges). Clearly, $\kappa_x \neq 0$ and $\epsilon_x^0 = \epsilon_y^0 = \gamma_{xy}^0 = \kappa_y = \kappa_{xy} = 0$. Hence, the in-plane strains along the principal material directions become

$$\left\{ \begin{array}{c} \epsilon_1 \\ \epsilon_2 \\ \gamma_{12}/2 \end{array} \right\}_k = \left[\begin{array}{c} zc^2 \\ zs^2 \\ -zcs \end{array} \right] \left\{ \kappa_x \right\} \tag{12}$$

where c and s are the cosine and sine of the ply angle for lamina k.

In an isotropic plate of thickness t, and also a laminated plate made from unidirectional plies and bent along its principal material direction, the maximum strain occurs on the outer edges of the plate, and hence at $z = \pm t/2$. It would seem natural to compare these peak bending strains with the ultimate strains for the fibres. However, extensive experiments on thin laminates made from woven CFRP composites ([4], [5]) have shown that these laminates are able to survive peak bending strains that are much larger than those obtained from the above approach. It is reasonable to assume that a woven lamina in bending fails when the strain at the *centre of the outermost yarn* reaches the ultimate value.

The minimum bend radii were estimated for laminated plates made of woven T300 carbon fibre in LTM45 epoxy resin. Two types of weaves were considered: 0.2 mm thick, 200 gsm 2 × 2 twill; and 0.11 mm thick, 94 gsm plain weave. The material properties of the composites are given in Table 1.

The estimated minimum bend radii for thin plates made from these materials are listed in Table 2, along with experimental data. The maximum strain criterion yields conservative results when compared to the experimental data.

Measurement of Minimum Bend Radius

Bending tests were carried out to measure the minimum radius of curvature prior to failure of the laminated plates listed above. Because of their small thickness, these plates can be bent into very small radii, and hence standard three-point and four-point bending tests are found to be unsuitable to measure the minimum bend radius. An alternative test that allows large displacements was devised, see Figure 9. Strip specimens with a width of 15 mm are attached to circular rods with a diameter of 15 mm, in turn connected to an Instron materials testing machine, using 50 mm long strips of 3M 79 tape. The specimens are $\pi R_i + 30$ mm long, where R_i is an initial estimate of the minimum radius of curvature, in order to ensure that failure takes place roughly in the configuration shown in the figure.

The tests were done with a cross-head speed of 5 mm/min, and were recorded with a Sony DCR-PC110E digital video camera. Once the specimen had failed, the minimum bend radius was measured using one or more images captured just before failure. If the specimen is too long, its ends come into contact prior to failure and in this case the test is repeated using a shorter specimen.

Results from this test are presented in Table 2. Note that the use of angle plies on the outer surfaces of the plate significantly decreases both the predicted and the measured minimum bend radius.

Table 1 Material properties of T300/LTM45

	2×2 twill	plain weave
E_1=E_2 (GPa)	65	56
G_{12} (GPa)	5	3
ν_{12}	0.06	0.05
V_f	0.55	0.48
$\epsilon_L^{(+)}$ (%)	1	1
$\epsilon_L^{(-)}$ (%)	1	1.1
ϵ_{LT} (%)	-	3.6
$S_L^{(+)}$ (MPa)	650	650
$S_L^{(-)}$ (MPa)	600	670
S_{LT} (MPa)	-	111

Table 2 Minimum bend radius of T300/LTM45 woven laminates.

					Predicted	Test
Material	Layup	Length (mm)	Width (mm)	Thickness (mm)	R_{min} (mm)	R_{min} (mm)
2x2 twill	0	62	15.0	0.2	5.0	4.0
2x2 twill	0/0	99	15.0	0.4	15.0	12.5
plain weave	0/45/0	85	14.3	0.33	13.7	10.4
plain weave	45/0/45	65	14.8	0.33	6.8	5.6

Sizing of Cut-outs in Side Walls

Cut-outs are required to reduce the maximum strain in the region where a hinge line crosses another hinge line in the same sheet of material. It is desirable for these cutouts to be as small as possible, to reduce the loss of stiffness of the structure. Stress concentrations near the edges of a cut-out in an airframe are usually avoided by reinforcing the structure in the immediate

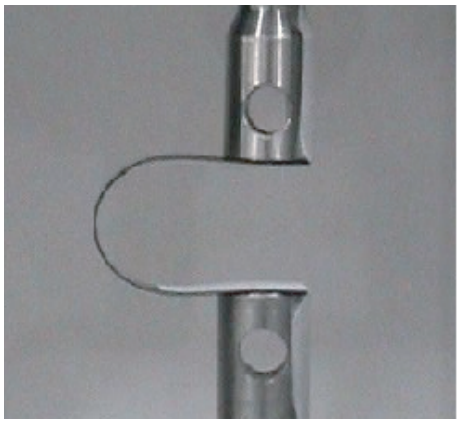

Fig. 9 Bending test for thin composites.

vicinity of the cut-out [6], which makes it thicker, but in the present case increasing the thickness of the side wall would actually increase the maximum stress. A rectangular shape (with rounded corners) of width w and length L was adopted, and only cut-outs for Z-folding were investigated in detail.

The width of the cut-out has to be such that the sidewall can be bent 180° along the "hinge line" H_1H_1, as shown in Figure 10(a). Hence, we need

$$w \geq \pi R_{min} \tag{13}$$

to prevent material failure, where R_{min} is the minimum bend radius of the side wall.

The length of the cut-out is determined by considering a longitudinal fold, about the line H_2H_2 in Figure 10(b), in the already flattened reflector structure. Assuming that the side walls and the RF surface have the same thickness and material properties, and hence the same minimum radius of folding R_{min}, the length of the cut-out can be estimated from

$$L \geq 2\pi R_{min} + \pi \mathrm{t} \tag{14}$$

Note that the part of the side wall that lies on the inside of the fold needs to bend first in one sense and then in the opposite sense. If the radius of curvature is assumed to be R_{min} everywhere, the inner part of the side wall would interfere with the outer part; however this can be eliminated by considering a fold with a non-uniform radius.

Design of Reflector Structure

Having established a methodology for ensuring that the reflector structure can be folded while remaining fully within the elastic range, two versions of the reflector were designed. The first version is a full-scale structure that provides the required parabolic surface and is designed for the flight loading environment. The second version is a half-scale structure that can be tested in the laboratory, under 1-g loading conditions, and requires only simple gravity compensation. The

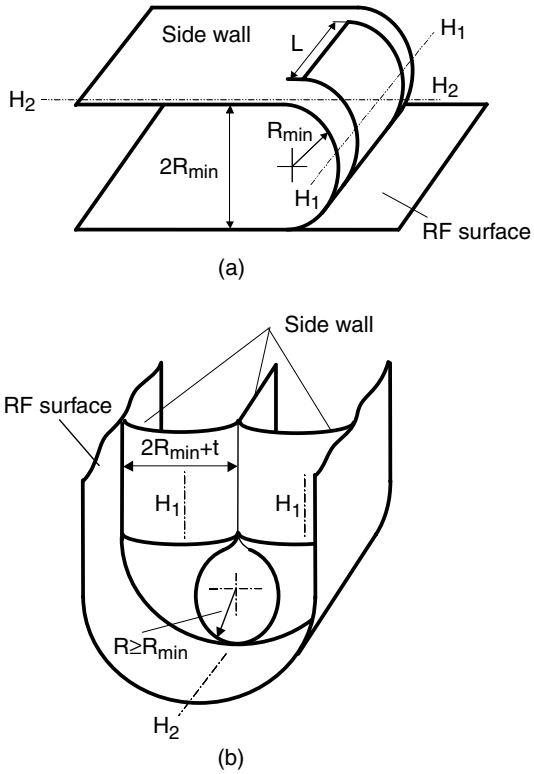

Fig. 10 (a) Folding of side wall about line H_1H_1 and (b) folding of RF surface around folded side wall.

geometry of this demonstrator is defined as an exact half-scale replica of the full-size reflector, e.g. the focal length is half, but is made from sheets of CFRP with the same wall thickness that would be used for the full-scale flight structure.

By designing two structures that have the same wall thickness, we ensure that the no scaling of the parts of the reflector that have to be folded elastically is required.

Structural Analysis of Deployed Reflector

The full-scale reflector structure was modelled with the ABAQUS finite element program [7]. The aim of the analysis was to study the static, dynamic, and buckling response of the structure, in the deployed configuration. First, the four surfaces that make up the structure were separately defined. Then, the structure was assembled by connecting the side walls along their edges to the RF surface and to the back surface. Both translational and rotational degrees of freedom were tied together along the connections.

It was assumed that the structure would be connected to the deployable truss shown in Figure 1, which in turn is connected to the spacecraft bus, through a rectangular interface frame attached to the first quarter of the RF surface. In the ABAQUS model it was assumed that the two longer sides of this rectangular frame have momentless connections to the RF

surface. A preliminary analysis showed that stiffening the ends of the structure with thin walled stiffeners increased the natural frequency of the structure significantly.

The material properties were based on a plain weave carbon T300/LTM45 laminate (0/45/0) with uniform thickness, see the section Prediction of Minimum Bend Radius for details. An inertial loading of 0.02 m/s^2 along the focal axis, i.e. the x-axis in Figure 6, was applied.

Different designs were compared by means of a multi-objective optimization performance criterion. This criterion was based on reducing the mass and increasing the deployed stiffness of the structure, and also increasing the safety margin against material and buckling failure. This optimization study showed that the best option had a wall thickness of 0.3 mm for all four surfaces, and symmetric side walls with end heights of 2 m. Non-symmetric designs of the side walls —leading to a tapered design of the reflector support structure— were also investigated, as it can be shown that such configurations can also be folded, but did not appear to be advantageous. The optimal structure had an overall mass of 29 kg, and the first natural frequency of 3.3 Hz. Hence, assuming that the connections would have a total mass of 15% of the main structural components, a total mass of 33 kg was estimated.

Having determined above the wall thickness of the full-scale structure, the laminate in the third row of Table 2 was selected, and hence R_{min} was set at 24 mm, which provides a margin of 2.3 on material failure, in the folded configuration.

A more detailed analysis of the half-scale demostrator was carried out. The finite element model of the demonstrator is shown in Figure 11, where the vector g denotes the direction of gravity. Note that each side wall has three windows whose dimensions are, from Equations 13 and 14, 210 mm long by 75 mm wide. The ends of the structure are stiffened by thin walled square section stiffeners (10 mm wide, 0.5 mm thick) made of the same material.

A preliminary analysis of the structure indicated that it was prone to buckle into a mode involving localised deformation of the upper part of the side wall, between the third cut-out and the tip. This mode was stiffened by attaching steel tape springs to both edges —for symmetry— of the side walls. Additional stiffening of the side walls was provided by attaching tape springs to the edges of all the cut-outs. The total mass of the demonstrator was estimated at 7.2 kg.

A contour plot of the displacement magnitudes due to gravity loading, assuming that the structure is held horizontally through four points at the corners of the interface frame, obtained from a linear static analysis are shown in Figures 12. Note that the maximum magnitude of displacement, 6.7 mm, occurs at the tip

Fig. 11 Finite element model of half-scale demonstrator.

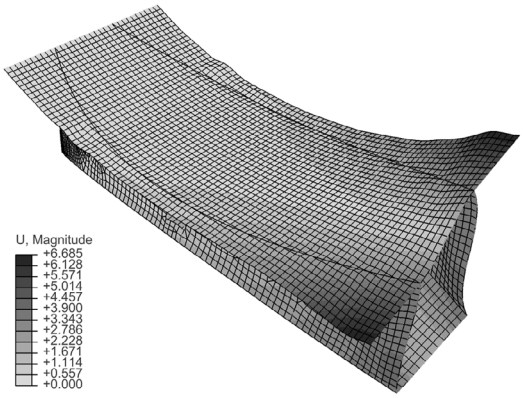

Fig. 12 Gravity-induced displacement magnitudes, in millimetres.

corners of the RF surface.

The margin against material failure, evaluated using the Tsai-Wu material failure criterion, was found to be huge, clearly indicating that excessive stresses are not an issue for the present structure (due to its very large "box" cross-section in the deployed configuration).

The first natural vibration mode, with a frequency of 6.8 Hz, resembles closely the gravity-induced deflections, see Figure 13.

The first buckling mode is shown in Figure 14. The factor of safety against buckling was 1.9.

Testing of Demonstrator

A detailed design of the demonstrator was then prepared; the CFRP sheets and angle stiffeners were constructed and water-jet cut by Brookhouse Paxford Ltd; all fixtures were made of Aluminium-alloy in the Workshops of the Engineering Department; the tape springs were made by cutting suitable lengths of Sears steel tape measure; 48 mm high cup-and-cone spacers made of a structural foam were made for the side walls, on either side of each hinge line; and all connections were made with 3M 79 woven-glass tape and 3M Scotch-Weld DP490 epoxy resin. The structure was

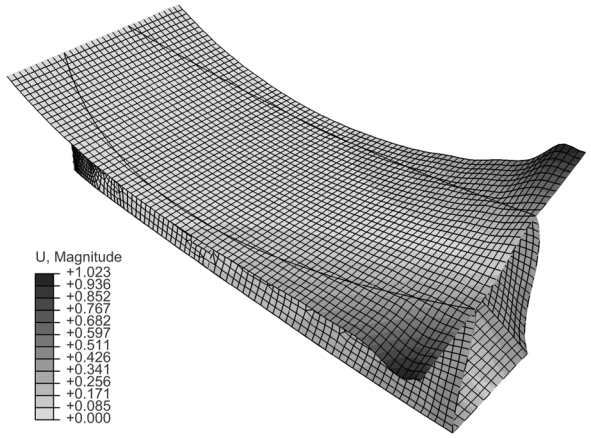

Fig. 13 First vibration mode (frequency=6.8 Hz)

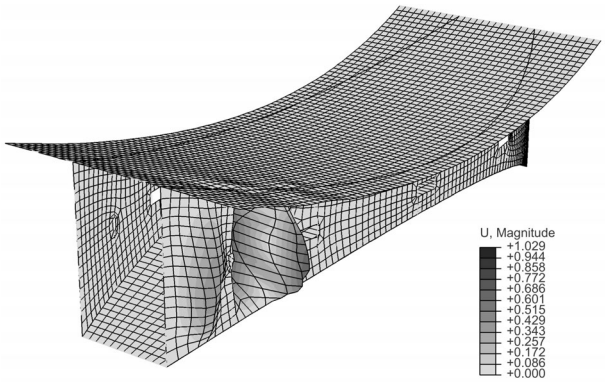

Fig. 14 First buckling mode.

then assembled in the the Deployable Structures Laboratory at Cambridge University. Its total mass was 11 kg, due to the mass, previously unaccounted for, of all spacers, washers, nuts and bolts, etc. Further details on the parts and assembly process are available in a technical report [2].

The reflector structure, see Figure 15, was attached through the interface frame to a tubular steel support structure, with a 2.5 kg single-point gravity offload at the root of the back surface, and a 4 kg offload connected to the top edge of the RF and back surfaces, through a horizontal bar.

Measurements of surface accuracy and stiffness were then taken, in the deployed configuration. The stiffness of the demonstrator was measured before packaging, whereas the surface accuracy was measured both before packaging and after deployment.

Measurements of Stiffness

Displacement measurements of the tip of the structure were carried out in the deployed configuration. These measurements were taken with a LK 081 (Keyence Co.) laser displacement sensor.

Static loads in the out-of-plane and transverse directions were applied to the tip of the reflector structure,

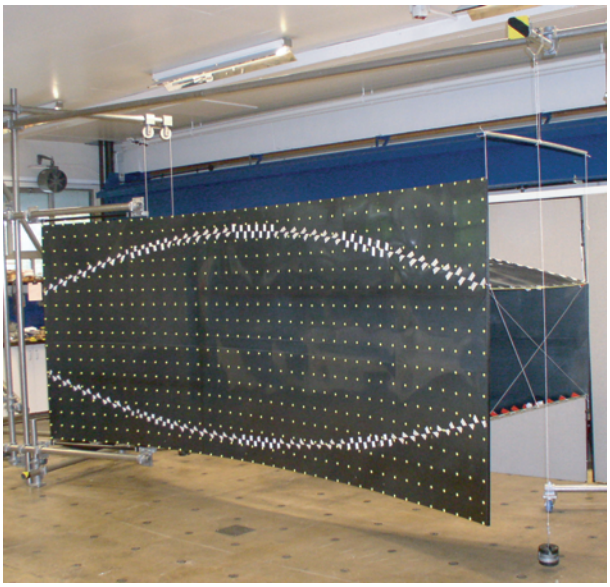

Fig. 15 Half-scale demonstrator attached to support rig and with gravity off-load at the tip.

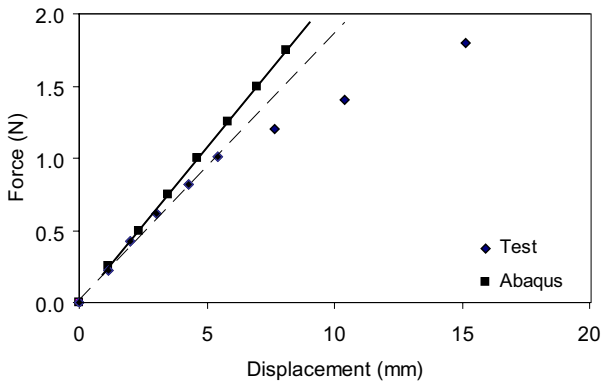

Fig. 16 Response to horizontal tip loads.

by means of a string and pulley system. The displacements in the direction of the load were measured in each test, and in each case a linear best-fit relationship was obtained, in order to estimate the stiffness of the structure for the both load cases. Figures 16 and 17 compare the measured response to the results from an ABAQUS linear-elastic static analysis. The ABAQUS model is stiffer in both cases, by 15% in the out-of-plane direction, and by 49% in the vertical direction.

Obviously, some refinement of the model (e.g. by measuring the actual elastic properties of the composite sheets and by modelling the support conditions in more detail) would be desirable. However, note that the out-of-plane stiffness of the structure, which is the lowest one, is in good agreement with the measurements.

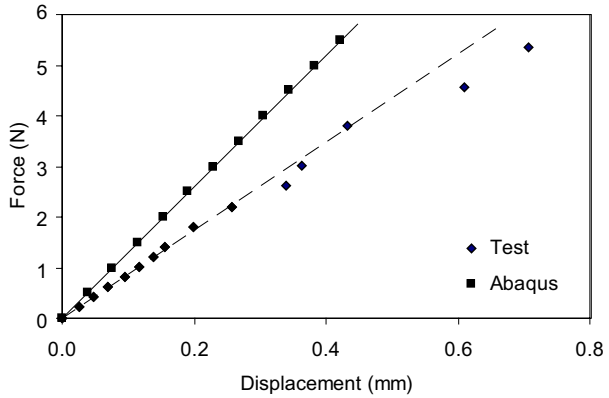

Fig. 17 Response to vertical tip loads.

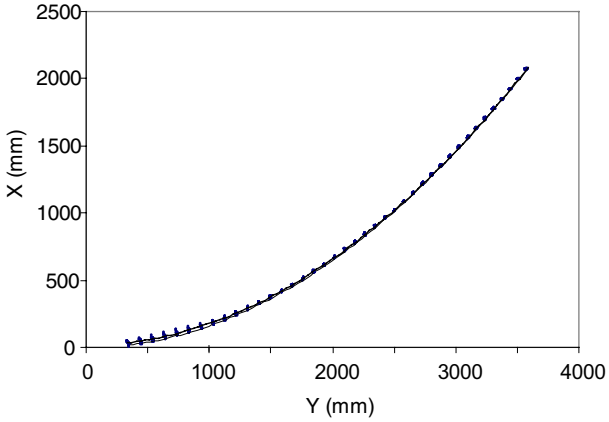

Fig. 18 Best fit parabolas, before and after packaging.

Measurement of Surface Accuracy

A PC based photogrammetry package, PhotoModeler Pro 4.0 [8], was used to measure the surface accuracy of the RF surface of the half-scale demonstrator. 680 circular, equally spaced targets, were attached to the surface. The measurements were carried out both before packaging the structure for the first time and after deploying it.

Since we are dealing with a parabolic cylinder, the problem is essentially in two dimensions. The z-coordinates of the target points, where z is perpendicular to the plane of the parabola, see Figure 6, can be disregarded. The equation of the best-fit parabola, in a coordinate system in which X and Y are parallel to x and y, respectively, and X_0 and Y_0 are the measured coordinates of the vertex of the parabola, is

$$X = \frac{1}{4a^*}Y^2 - \frac{Y_0}{2a^*}Y + \left(X_0 + \frac{Y_0^2}{4a^*}\right) \qquad (15)$$

Note that, once the best fit parabola in Eq. 15 has been obtained, the focal length is a^*.

For n target points that are equally spaced on the surface, the root mean square (RMS) error in the axial direction X, with respect to the best fit parabola, is calculated from [9]

$$\delta_{ex} = \sqrt{\frac{\sum(\hat{X}_i - X_i)^2}{n}} \qquad (16)$$

where $\hat{X}_i$ is the axial coordinate of a general target point and X_i is the corresponding axial coordinate of the best fit parabola.

Figure 18 shows the best fit parabolas, before and after packaging. Before packaging, the best-fit focal length was $a^* = 1550$ mm, which is very close to the design focal length of $a = 1544.5$ mm. The RMS error of the target points from the best fit parabola was 3.8 mm. It was noticed that the points near the upper edge of surface, between the two stiffeners that form the longer edges of the interface frame, yielded higher errors. It was thus realised that the interface frame and the RF surface had not been not correctly aligned during assembly. When these points, which correspond to 6% of the surface area, were excluded from the calculations, the RMS error reduces to 3.3 mm.

The surface accuracy measurements were repeated after packaging and deployment of the structure. The best-fit focal length was 1547.1 mm. The total RMS error from the best fit parabola was 5.1 mm, and disregarding the same target points near the interface frame as above reduced the error to 4.0 mm.

Packaging and Deployment of the Demonstrator

Packaging

Packaging consists in flattening the structure and then introducing three transverse folds that allow it to fold into an accordion. The folding sequence is shown in Figure 19.

Flattening the structure involves bending the side walls through 180°. The process through which this happens needs to be carefully controlled, to prevent damaging the structure. First, the demonstrator was placed on a plywood mold, with the RF surface facing down and the back surface facing up. Foam plugs that fit snugly inside the "hollow solid" were placed inside the structure to prevent it from suddenly collapsing. Easy-release cable ties were passed through corresponding sets of cup-and-cone spacers, and were tied to take up any slack.

Next, flattening of the structure was initiated by pulling the side walls outwards with a pair of wooden poles placed inside the structure, between the sets of cup and cone spacers. Each pole was loaded, through a cable and pulley system, with counter weights, while the foam plugs were slowly pulled out to allow the back surface to come down.

Note that as the structure flattens the back surface and the RF surface need to move symmetrically, respectively up and down, to keep the longitudinal fold lines in the sidewalls straight and horizontal. To

ensure this, plywood sheets were gradually pushed between the mold and the structure, and slowly raised at the far ends, to move the RF surface upwards.

It was discovered that the structure has a tendency to "roll-over", i.e. to slew sideways during folding. This is avoided by cross-bracing both ends with cable ties attached to adjustable plastic ties, which are held taut at all times. Also, two people had to hold the upper ends of the back surface.

Once the back surface had stopped coming down under its own weight, weights were added on top of expanded polystyrene sheets to bring the back surface down. Throughout this process the easy release cable ties were progressively tightened to take up any slack, and the foam plugs were gradually pulled out from either end. Once the demonstrator had substantially flattened, plastic ties were introduced at 150 mm spacing along the fold line of the side walls.

Longitudinal folding is much simpler than flattening. First, the two end sections are rotated through 180°, making sure that the RF surface ends up on the outside, and then the middle fold is introduced, this time placing the RF surface on the inside.

Figure 20 shows the the packaged structure, whose outer envelope is 1700 mm long, 950 mm wide,and 260 mm high. Note that the packaged envelope of the full-scale, flight structure would have the same height, but double the length and width.

Deployment

The strain energy stored in the packaged demonstrator was too large for the structure to be allowed to deploy dynamically, by releasing its longitudinal constraints and then the transverse constraints. Instead, an operator assisted deployment was carried out.

The packaged structure was attached to the tubular steel support structure, through the corners of the rectangular interface frame. The structure was then deployed under quasi-static conditions, in two stages, with gravity supports provided along the three transverse fold lines.

The photographs at the start of the sequence in Figure 21 show the first stage of the deployment process, in which the structure deploys as an accordion and ends up flat. Friction in the gravity offload system held the structure in equilibrium in any of its intermediate configurations.

Once the first stage of the deployment process had been completed, the side walls were allowed to unfold by gradually releasing the cable ties, thus separating the RF surface from the back surface. The structure was cross-braced at both ends to prevent it from slewing.

Fig. 19 Packaging sequence, from top left to bottom right.

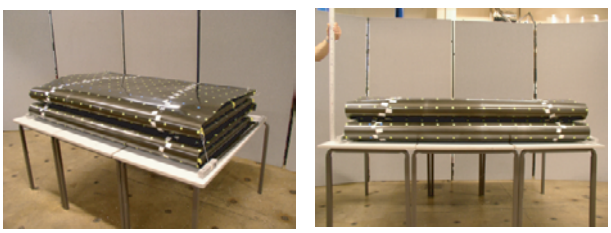

Fig. 20 Packaged demonstrator.

Conclusion

An innovative concept for large deployable reflectors for synthetic aperture radar applications has been pre-

Fig. 21 Deployment sequence, from top left to bottom right.

sented. This concept can deliver a parabolic profile of high accuracy with a structure of very low mass, high stiffness, and potentially very low cost.

At full scale, i.e. for a reflecting surface that is 7.9 m long and 3.2 m wide, it has been estimated that the proposed approach would lead to a structure weighing about 33 kg, which is two-and-half times lighter than a traditional reflector structure made from lightweight, curved panels with self-locking hinges.

The new concept is based on forming a collapsible hollow solid, defined by four cylindrical surfaces. These surface are formed from thin-walled CFRP sheets hinged along their edges. This is just one particular approach, and it should be noted that there are many other ways of implementing this type of structural concept. Patent applications protecting the new concept presented in this paper have been filed [10].

The key to forming a cylindrical surface with the required shape lies in the cutting pattern for the edges of the sheets. A general methodology for determining the cutting pattern has been presented, and for the case of parabolic shapes an analytical expression for the cutting pattern has been obtained, in terms of the focal length, aperture and offset distance of the reflector.

The proposed concept has been demonstrated by designing, constructing and testing a half-scale physical demonstrator made from 0.3 mm thick CFRP sheets, which would also be used for the full-scale structure. This model has achieved a surface accuracy of 3.8 mm RMS, typical mass of 1.7 kg/m^2, typical deployed frequency of 6.8 Hz, and packaging density of 1/16th of deployed volume.

Acknowledgments

This research was funded by EADS Astrium Ltd, under the BNSC Newton scheme. The authors are grateful to Mr Mark Roe, whose vision has made this work possible, and Mr Phil Howard —both of EADS Astrium— for substantially contributing to the new concept and its implementation. The authors thank Mr Tony Di Pasquale of Brookhouse Paxford, Ltd and Mr Peter Knott of Cambridge University for technical support.

References

[1]Watt, A.M., Pellegrino S., Tape-Spring Rolloing Hinges, Proceedings of 36th Aerospace Mechanisms Symposium, Glenn Research Center, May 15-17, 2002.

[2]Soykasap, Ö., Pellegrino S., Deployable Synthetic Aperture Radar Reflector, CUED/D-STRUCT/TR209, Department of Engineering, University of Cambridge, 2004.

[3]Gibson, R.F., Principals of Composite Material Mechanics, McGraw-Hill Book Co., Singapore, 1994.

[4]Yee, J.C.H, and Pellegrino S., Folding of Composite Structures, Submitted to *Composites/A*, 2003.

[5]Gerngross, T., Folding of Thin-Walled Composite Structures, Technical University of Munich, Munich TUM-MW 65/0331-SA, 2003.

[6]Niu M.C., Airframe Structural Design, Conmilit Press Ltd, Hong Kong, 1990.

[7]Hibbit, Karlsson and Sorensen,Inc., ABAQUS/Standard User's Manual, Version 6.2., Pawtucket, RI, USA, 2001.

[8]PhotoModeler Pro 4.0, User Manual, Eos Systems Inc, Canada, 2000.

[9]Levy, R., Structural Engineering of Microwave Antennas, The Institute of Electrical and Electronics Engineers, New York, 1996.

[10]Watt, A.M., Pellegrino S., Howard, P., Improvements Relating to a Deployable Support Structure, Patent Applications: UK-GB0316734.3, European-EP03254474.4, 2003.